

FAINT OBJECT SPECTROGRAPH OBSERVATIONS OF THE LOW-LUMINOSITY SEYFERT GALAXY NGC 1566

G. A. KRISS,¹ G. F. HARTIG,² L. ARMUS,¹ WILLIAM P. BLAIR,¹ S. CAGANOFF,¹ AND L. DRESSSEL³

Received 1991 May 1; accepted 1991 May 15

ABSTRACT

FOS observations of the Seyfert galaxy NGC 1566 show it to possess the broad lines characteristic of a typical Seyfert 1 galaxy, even in states of very low luminosity. The continuum, however, is steep ($f_\nu \sim \nu^{-1.5}$) with no suggestion of the ultraviolet excess seen in higher luminosity AGNs. The broad emission lines have symmetric profiles, but are redshifted by 200–1000 km s⁻¹ relative to the systemic velocity. The broad-line ratios indicate a low ionization parameter, and the strength of lines such as Fe II, Mg II, and the Balmer continuum relative to the UV continuum supports models for X-ray heating of the broad-line cloud interiors.

The sharp core of the *HST* point response function gives a significant advantage over ground-based telescopes for observations of low luminosity active galaxies, despite the spherical aberration of the primary mirror. The high contrast of the active nucleus over the surrounding starlight permits observers to use the small apertures of the FOS to reject most of the contaminating starlight that frustrates ground-based observations and to obtain nearly simultaneous spectra spanning the full UV and optical wavelength range.

Subject headings: galaxies: individual (NGC 1566) — galaxies: nuclei — galaxies: Seyfert — ultraviolet: spectra

1. INTRODUCTION

Many apparently “normal” galaxies exhibit low levels of nuclear activity (e.g., Keel 1983; Filippenko & Sargent 1985). It is important to determine how this low-level activity is related to that in more luminous active galaxies, and if they involve similar mechanisms of energy generation and emission line formation. Ground-based studies of weak nuclear activity are often frustrated by the large starlight contamination from the surrounding galaxy that is unavoidable in slits of $\sim 2''$. In spite of the spherical aberration in its primary mirror, the sharp core of the *Hubble Space Telescope* (*HST*) point response function makes it possible to study high contrast objects such as active galactic nuclei at fairly high angular resolution. With the small apertures of the Faint Object Spectrograph (FOS) on *HST*, one can reject most of the starlight and obtain nearly simultaneous spectra of the full UV through optical wavelength range.

NGC 1566 is a nearby Seyfert 1 Galaxy that spends most of its time in low-luminosity states where the broad permitted lines are nearly undetectable (Alloin et al. 1986). The narrow lines have ratios more similar to those of Seyfert 2 galaxies than Seyfert 1 galaxies (Alloin et al. 1985), and Hawley & Phillips (1981) comment that, aside from the weak broad-line emission, the nuclear spectrum more closely resembles a giant H II region than a Seyfert galaxy. Hence, despite its small distance ($13.0h^{-1}$ Mpc for $cz_\odot = 1504$ km s⁻¹; Pence, Taylor, & Atherton 1990), NGC 1566 was not recognized as an active galaxy until the broad lines and strong blue continuum characteristic of Seyfert 1 galaxies were noticed by Shobbrook (1966) during an interval of high activity. The clear Seyfert 1 characteristics of NGC 1566 in its high state and its similarity to other weakly active galaxies in low states make it an excellent

transitional object for studying the physical conditions in a low-level active nucleus for comparison to more typical active galaxies. We therefore obtained spectra of the nucleus of NGC 1566 through the 0.3 circular aperture of the FOS on *HST* during a typical low-luminosity interval.

2. OBSERVATIONS AND DATA REDUCTION

FOS spectra of NGC 1566 using gratings G270H, G400H, and G570H on the FOS red side were obtained on 1991 February 8. For each spectrum eight separate readouts were made at 250 s intervals for total exposures of 2000 s. The internal Pt-Cr/Ne calibration lamp was observed immediately following the G570H integration as a check on the wavelength calibration. Blue side spectra using gratings G130H and G190H were obtained on 1991 February 11. Two separate exposures of 2000 s were made on successive orbits for each grating. The spectra have a resolution of ~ 250 km s⁻¹.

Acquisitions were designed to center the active nucleus in the 0.3 aperture using successive peak-ups in the 4'3, 1'0, 0'5, and 0'3 apertures (Kinney & Ford 1990). The final peak-up on both the red and blue side acquisitions was in one corner of the scan pattern, but judging from the relative numbers of counts in the adjacent pointings, we estimate that the nucleus was centered to better than 0'05 for each set of observations. The good agreement in flux levels in the region of wavelength overlap between grating G190H on the blue side and grating G270H on the red side (better than 8%) supports our confidence in the pointing accuracy.

The raw data were processed to remove most of the effects of the geomagnetically induced image motion (Junkkarinen et al. 1991) by computing the expected shift in the dispersion direction for each integration/readout period, then offsetting the spectra by integral quarter-diode steps to compensate before adding. Background rates (predominantly induced by charged particles) were computed from a model that accounts for the dependence on geomagnetic latitude and then subtracted. To compensate for the additional contribution of grating-scattered light to the background of the G130H spectrum, we

¹ Center for Astrophysical Sciences, Department of Physics and Astronomy, The Johns Hopkins University, Baltimore, MD 21218.

² Space Telescope Science Institute, 3700 San Martin Drive, Baltimore, MD 21218.

³ Applied Research Corporation, 8201 Corporate Drive, Suite 1120, Landover, MD 20785.

subtracted the mean count rate measured below the 1150 Å cutoff of the blue detector. The spectra were corrected for small-scale photocathode nonuniformities using flat-fields developed from observations of the standard star G191B2B.

Conversion to absolute flux was performed by multiplying the count rates by inverse sensitivity curves representing the mean reduction of three (blue side) or four (red side) standard star spectra. Correction for losses at the 0.3 aperture (which amount to more than 80% of the light in a point source image due to the degraded point spread function) was based on the relative aperture throughput determined from observations of 3C 273 (Bahcall et al. 1991). The nominal wavelength scales of all spectra except G570H were determined from on-board calibration lamp observations during the orbital verification testing period. Small zero point corrections were applied to the G130H spectra based on the position of the geocoronal Ly α emission line and to the G270H spectrum using measurements of interstellar Mg II and Fe II lines. The Pt-Cr/Ne lamp exposure following the G570H spectrum was used to set its wavelength scale, and the G400H spectrum was fixed relative to the

G570H data using the He II λ 4686 line, which appears in both spectra. Figure 1 shows calibrated spectra covering the wavelength range 1150–6820 Å. Identified emission and absorption features are indicated. The G130H and G190H spectra have been smoothed with a Gaussian with a full width at half-maximum of 1 diode, approximately the instrumental resolution, while the other spectra are shown unsmoothed.

Fluxes, line centers, and line widths in the NGC 1566 spectra were determined by fitting multiple Gaussian components to the emission lines with a nonlinear χ^2 minimization technique. We always chose the minimum number of components required to produce an acceptable fit, typically two Gaussians for the narrow lines and a single Gaussian for the broad lines. The Ly α line in our spectrum is distinctly asymmetric, unlike the other broad lines. The asymmetry appears to be caused by absorption by neutral hydrogen along the line of sight. In our fit we have allowed for damped Ly α absorption, and the broad- and narrow-line fluxes are our best estimate of the intrinsic flux. The correction for absorption amounts to 61% of the narrow line flux, and 58% of the broad line flux. In Table 1 we

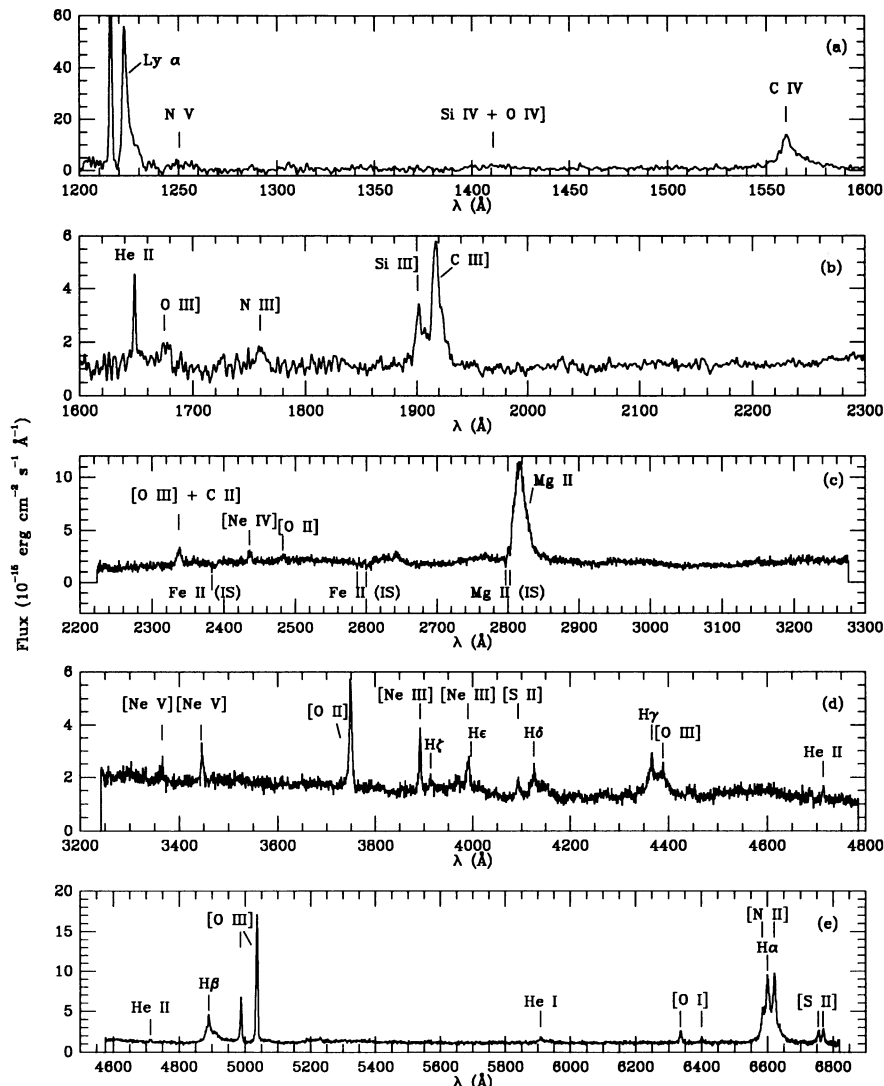


FIG. 1.—(a–e) The spectra of NGC 1566 obtained with the FOS on *HST* using gratings G130H and G190H on the blue side, and gratings G270H, G400H, and G570H on the red side. The G130H and G190H spectra have been smoothed with a Gaussian of FWHM = 1 diode, approximately the resolution of each spectrum. Geocoronal Ly α is off scale in panel (a).

TABLE 1
EMISSION LINES IN NGC 1566

Line	λ_{vac} (Å)	Flux (10^{-15} ergs cm^{-2} s^{-1})	cz_{\odot} (km s^{-1})	FWHM (km s^{-1})
Ly α n	1215.67	282.20 \pm 74.95	1708 \pm 66	431 \pm 131
Ly α b	1215.67	259.90 \pm 71.46	1855 \pm 296	2376 \pm 626
C IVb	1549.05	104.10 \pm 16.27	2665 \pm 240	3230 \pm 561
O III]	1663.00	7.40 \pm 2.79	2162 \pm 356	1588 \pm 670
Si III]n	1892.03	4.45 \pm 3.61	1418 \pm 259	575 \pm 485
Si III]b	1892.03	13.31 \pm 5.57	1791 \pm 405	1719 \pm 762
C III]n	1907.49	12.66 \pm 3.96	1433 \pm 127	705 \pm 211
C III]b	1908.73	33.61 \pm 6.09	1597 \pm 196	2039 \pm 418
Mg IIb	2799.50	191.30 \pm 6.15	1816 \pm 42	2489 \pm 85
[O II]	3727.10	14.46 \pm 0.35	1629 \pm 12	394 \pm 0
[O II]	3729.90	12.33 \pm 0.34	1646 \pm 12	394 \pm 0
H γ n	4341.68	4.93 \pm 1.01	1661 \pm 46	402 \pm 0
H γ b	4341.68	30.96 \pm 2.50	2304 \pm 46	2523 \pm 0
[O III]	4364.50	2.62 \pm 0.35	1682 \pm 60	394 \pm 0
H β n	4862.68	16.58 \pm 2.82	1674 \pm 41	437 \pm 94
H β b	4862.68	64.64 \pm 5.87	2390 \pm 132	2583 \pm 256
[O III]	4960.30	35.77 \pm 4.28	1623 \pm 27	394 \pm 0
[O III]	5008.20	101.63 \pm 7.32	1629 \pm 14	394 \pm 27
H α n	6564.61	42.96 \pm 5.44	1595 \pm 30	402 \pm 62
H α b	6564.61	211.18 \pm 11.58	2052 \pm 60	2342 \pm 127
[S II]	6718.30	12.28 \pm 2.22	1603 \pm 35	353 \pm 77
[S II]	6732.70	13.80 \pm 2.24	1606 \pm 30	333 \pm 58

give total line fluxes, mean heliocentric redshifts, and integrated profile widths. The $\Delta\chi^2$ used for the 1σ confidence intervals was determined as prescribed by Avni (1976). Error bars were then calculated using the covariance matrix of the fit scaled by the reduced χ^2 (Bevington 1969). The tabulated errors represent only statistical errors and do not take any systematic calibration errors into account. Error bars set equal to zero in Table 1 indicate a parameter that was fixed at the given value.

The UV and optical multiplets of Fe II are prominent in our spectra over the 2000–5500 Å wavelength range; their strength makes setting the continuum levels particularly difficult, so we adopted a strategy of fitting a synthesized Fe II spectrum simultaneously with the continuum over this wavelength range. Planetary Camera (PC) images through the F547M filter (Kriss et al. 1990) also show that starlight from the $\sim 1''$ bulge of NGC 1566 should contribute 32% of the flux through a 0.3 circular aperture. Our continuum model consists of a power law with $F_{\lambda} = F_0(\lambda/1000 \text{ Å})^{-\alpha}$, a G8 III stellar spectrum fixed at 32% of the 5470 Å continuum, the Fe II UV and optical multiplets (Netzer & Wills 1983; Wills, Netzer, & Wills 1985) convolved with a Gaussian of FWHM of 2500 km s^{-1} (the width of broad H β in our spectrum), an optically thin Balmer continuum, and extinction following the mean galactic curve of Seaton (1979). The intensities of the UV and optical multiplets of Fe II are permitted to vary independently. The best fit is obtained for $F_0 = 1.91 \pm 0.03 \times 10^{-15}$ ergs cm^{-2} s^{-1} Å $^{-1}$, $\alpha = 0.47 \pm 0.01$, $E_{B-V} \pm 0.062 \pm 0.002$, a Balmer continuum flux of $1.3 \pm 0.04 \times 10^{-12}$ ergs cm^{-2} s^{-1} at $T = 11,590 \pm 450$ K, a flux of $9.27 \pm 0.45 \times 10^{-13}$ ergs cm^{-2} s^{-1} in the UV Fe II lines, and a flux of $3.82 \pm 0.29 \times 10^{-13}$ ergs cm^{-2} s^{-1} in the optical multiplets. We allowed for the possibility of a second, bluer continuum component representative of a hot accretion disk; such a model requires much higher extinction and gives unacceptably large χ^2 .

3. DISCUSSION

Despite the low luminosity of the nucleus of NGC 1566 at the time of our observations, the continuum in our spectra is dominated by nonthermal emission. The stellar features in the spectra of Alloin et al. (1985) are conspicuously absent from our FOS spectra. The 32% starlight fraction at 5470 Å through a 0.3 aperture measured from our PC images (Kriss et al. 1990) may be compared to the $\sim 70\%$ starlight fraction in Figure 1 of Alloin et al. (1985) when the continuum was 2–3 times brighter than our observations. While the 0.3 aperture of the FOS admits only $\sim 20\%$ of the light from a point source, the contribution from diffuse starlight is suppressed by nearly two orders of magnitude relative to typical ground-based observations through apertures of $\sim 2''$ square. This enables us to achieve an order of magnitude improvement in the ratio of nuclear flux to contaminating starlight, despite the deleterious effects of the spherical aberration in the primary mirror. With the broad wavelength coverage of the FOS we obtain a clear picture of the continuum with nearly simultaneous spectra over the full UV and optical wavelength range, and the uncertainties in matching ground-based optical observations with different apertures to space-based UV observations are avoided. We note, however, that the advantages of the FOS in rejecting starlight relative to ground-based instruments will be significantly less if the starlight is unresolved (e.g., NGC 7457; Lauer et al. 1991).

While many active galaxies have large UV excesses that are attributed to thermal emission from an accretion disk (Malkan & Sargent 1982; Malkan 1983), the UV excess is not always present. In its lack of a UV excess, NGC 1566 is similar to NGC 4151 (Malkan & Sargent 1982), and its steep continuum resembles the redder spectra seen at low luminosity in other variable AGN (Edelson et al. 1990; Clavel et al. 1991). The bluer emission seen in the high-luminosity states of other AGN may be increased thermal emission from the accretion disk (Krolik et al. 1991). We conclude that thermal radiation from an accretion disk contributes little to the energetics of NGC 1566 at low luminosity.

To estimate the density and temperature of the narrow-line region we employ the usual astrophysical plasma diagnostics. For the [S II] doublet we measure an intensity ratio $I(\lambda 6716)/I(\lambda 6731) = 0.89 \pm 0.22$ which implies a density of 830_{-120}^{+320} cm^{-3} (Osterbrock 1989). Deblending the [O II] doublet yields an intensity ratio $I(\lambda 3729)/I(\lambda 3727) = 0.85 \pm 0.12$ with a corresponding density of 710_{-140}^{+200} cm^{-3} (Osterbrock 1989). Both are in good agreement with the measurements of Alloin et al. (1985). The [O III] line ratios $[I(\lambda 4959) + I(\lambda 5007)]/I(\lambda 4363) = 53.4 \pm 8.5$ and imply a relatively high temperature of $17,200_{-1300}^{+1700}$ K (Osterbrock 1989). The intensity of $\lambda\lambda 1661, 1666$ relative to $\lambda\lambda 4959, 5007$ is consistent with this measurement (Keenan & Aggarwal 1987), but the errors are much larger. The high temperature estimate should be viewed with caution, however, since Aldrovandi & Gruenwald (1985) show that physical conditions prevailing in AGN narrow-line regions favor mechanisms that can elevate the observed ratios of [O III] $\lambda\lambda 4363$ to $\lambda\lambda 4959, 5007$. We add the additional caveat that these line ratios may represent an average of regions of different temperatures and densities rather than a uniform gas, in which case the plasma diagnostics are meaningless. In fact, the unusually strong narrow-line emission from Si III suggests there may be a fairly high density component to the narrow-line region. The high ratio of Si III] $\lambda 1892$ to [Si III] $\lambda 1882$

requires densities of 10^5 cm^{-3} or more (Nussbaumer 1986). The high intensity of Si III] $\lambda 1892$ relative to C III] $\lambda 1909$ is also indicative of high densities (Feibelman & Aller 1987).

All broad-line components are well fitted by single, symmetric Gaussian profiles. The line centers, however, are redshifted from the systemic velocity by 200–1000 km s^{-1} with a weak correlation between line width and redshift. Redshifts of comparable magnitude are seen in other AGN (Peterson, Crenshaw, & Meyers 1985; Peterson 1987). They may be indicative of gravitational redshifts (Netzer 1977), but the required black hole mass and BLR radius are incommensurate with probable values for NGC 1566 (Alloin et al. 1986). Asymmetries can also be induced by the outflow of optically thick clouds (Ferland et al. 1979); Capriotti, Foltz, & Byard 1979), or by infalling clouds with the far side of the BLR obscured from view. The several hundred km s^{-1} redshifts in NGC 1566 are compatible with free fall velocities in the potential of a black hole of mass $5 \times 10^6 M_{\odot}$ at a radius of $3 \times 10^{16} \text{ cm}$ (Alloin et al. 1986). The positive correlation between width and redshift implies that broader lines would arise from infalling clouds closer to the black hole, similar to the correlation between line width and cross-correlation lag time seen for broad lines in NGC 5548 (Krolik et al. 1991).

The energy budget of the BLR support models in which the Fe II multiplets, the Balmer lines and continuum, and a significant fraction of Mg II $\lambda 2798$ are formed at high optical depths inside the broad-line clouds in a partially ionized zone that is heated by kilovolt X-radiation (e.g., Kwan & Krolik 1981). We find a total reddening-corrected flux in Fe II multiplets, Mg II, and the Balmer continuum of $2.8 \times 10^{-12} \text{ ergs cm}^{-2} \text{ s}^{-1}$. This exceeds the reddening-corrected total UV flux of $2.4 \times 10^{-12} \text{ ergs cm}^{-2} \text{ s}^{-1}$ in our extrapolated power law-continuum from 13.6 to 136.0 eV, implying that the UV continuum cannot supply the required energy. An absorption-corrected X-ray flux of $9.3 \times 10^{-12} \text{ ergs cm}^{-2} \text{ s}^{-1}$ was seen in an *Einstein* Imaging Proportional Counter observation on 1979 September 20 (Kruper et al. 1990). The broad H β flux at this epoch was $\sim 50\%$ higher than our observed flux (Alloin et al. 1986); scaling down the X-ray flux proportionately gives $6.5 \times 10^{-12} \text{ ergs cm}^{-2} \text{ s}^{-1}$. This is adequate to power the Fe II lines, Mg II,

and the Balmer continuum emission with a covering factor of 40%. The flux in the remaining broad lines totals $5.2 \times 10^{-13} \text{ ergs cm}^{-2} \text{ s}^{-1}$, within the energy budget of the UV continuum for a comparable covering factor.

The strong Mg II $\lambda 2798$ and C III] $\lambda 1909$ emission observed relative to C IV $\lambda 1549$ and Ly α are indicative of a low ionization parameter. Broad Si III] $\lambda 1892$ is also unusually strong. Just as C III] $\lambda 1909$ brightens rapidly relative to C IV $\lambda 1549$ at low ionization parameters, Si III] $\lambda 1892$ should brighten relative to Si IV $\lambda 1400$, which is very weak in the G130H spectrum, again suggesting a low ionization parameter. Comparison of our line ratios to grids of models in Mushotzky & Ferland (1984) and Krolik & Kallman (1988) suggests a density of $\log N \sim 10$ and an ionization parameter of $\log U = -2.4$ to -3.0 (where U is the ratio of ionizing photon density to electron density) as deduced by Alloin et al. (1986), but no single set of parameters matches all line ratios. The steep UV spectrum and relatively strong X-ray emission we infer from the low-density state of NGC 1566 is very different from the assumed spectrum in any of these models, and this may account for many of the differences.

In summary, the sharp core of the *HST* point response function and the high contrast of an unresolved active nucleus over the surrounding starlight permits observers to use the small apertures of the FOS to reject most of the contaminating starlight in low-luminosity AGNs. Our spectra of the Seyfert galaxy NGC 1566 clearly show the broad lines and nonthermal continuum characteristic of Seyfert 1 galaxies, even in a state of very low luminosity. The continuum, however, is steep ($f_{\nu} \sim \nu^{-1.5}$) with no suggestion of the ultraviolet bump seen in higher luminosity AGN. The broad emission lines have symmetric profiles but are redshifted by several hundred km s^{-1} relative to the systemic velocity. The broad line ratios indicate a low ionization parameter. The unusual strength of lines such as Fe II, Mg II, and the Balmer continuum supports models for X-ray heating of the broad line cloud interiors.

We acknowledge helpful discussions with H. Ford and R. Harms, and we thank J. Perelmutter for help with the figure. This work was supported by NASA contract NAS 5-29293.

REFERENCES

- Aldrovandi, S. M. V., & Gruenwald, R. B. 1985, *A&A*, 147, 331
 Alloin, D., Pelat, D., Phillips, M., Fosbury, R. A. E., & Freeman, K. 1986, *ApJ*, 308, 23
 Alloin, D., Pelat, D., Phillips, M., & Whittle, M. 1985, *ApJ*, 288, 205
 Avni, Y. 1976, *ApJ*, 210, 642
 Bahcall, J., et al. 1991, *ApJ*, 377, L5
 Bevington, P. 1969, *Data Reduction and Error Analysis for the Physical Sciences* (New York: McGraw Hill), 254
 Capriotti, E., Foltz, C. F., & Byard, P. 1979, *ApJ*, 230, 681
 Clavel, J., et al. 1991, *ApJ*, 366, 64
 Edelson, R. A., Krolik, J. H., & Pike, G. F. 1990, *ApJ*, 359, 86
 Feibelman, W. A., & Aller, L. A. 1987, *ApJ*, 319, 407
 Ferland, G. J., Netzer, H., & Shields, G. A. 1979, *ApJ*, 232, 382
 Filippenko, A. V., & Sargent, W. L. W. 1985, *ApJS*, 57, 503
 Hawley, S. A., & Phillips, M. M. 1980, *ApJ*, 235, 783
 Junkkarinen, V. T., Beaver, E. A., Cohen, R. D., Hier, R., Lyons, R., & Rosenblatt, E. 1991, *BAAS*, 22, 1283
 Keel, W. C. 1983, *ApJ*, 269, 466
 Keenan, F. P., & Aggarwal, K. M. 1987, *ApJ*, 319, 403
 Kinney, A. L., & Ford, H. C. 1990, *FOS Target Acquisition Handbook*, Version 2.1 (Baltimore: STScI)
 Kriss, G. A., et al. 1990, *BAAS*, 22, 1280
 Krolik, J. H., Horne, K., Kallman, T. R., Edelson, R. A., & Kriss, G. A. 1991, *ApJ*, 371, 541
 Krolik, J., & Kallman, T. 1988, *ApJ*, 324, 714
 Kruper, J. S., Canizares, C. R., & Urry, C. M. 1990, *ApJS*, 74, 347
 Kwan, J., & Krolik, J. H. 1981, *ApJ*, 250, 478
 Lauer, T. R., et al. 1991, *ApJ*, 369, L41
 Malkan, M. A. 1983, *ApJ*, 268, 582
 Malkan, M. A., & Sargent, W. L. W. 1982, *ApJ*, 254, 22
 Mushotzky, R., & Ferland, G. J. 1984, *ApJ*, 278, 558
 Netzer, H. 1977, *MNRAS*, 181, 89P
 Netzer, H., & Wills, B. J. 1983, *ApJ*, 275, 445
 Nussbaumer, H. 1986, *A&A*, 155, 205
 Osterbrock, D. E. 1989, *Astrophysics of Gaseous Nebulae and Active Galactic Nuclei* (Mill Valley, CA: University Science Books), 119
 Pence, W. D., Taylor, K., & Atherton, P. 1990, *ApJ*, 357, 415
 Peterson, B. M. 1987, *ApJ*, 312, 79
 Peterson, B. M., Crenshaw, D. M., & Meyers, K. A. 1985, *ApJ*, 298, 283
 Seaton, M. J. 1979, *MNRAS*, 187, 75P
 Shobbrook, R. 1966, *MNRAS*, 131, 293
 Wills, B. J., Netzer, H., & Wills, D. 1985, *ApJ*, 288, 94